Editors' Suggestion

Dropping mortality by increasing connectivity in plant epidemics

Ignacio Taguas,[*] José A. Capitán,[†] and Juan C. Nuño[‡]
Department of Applied Mathematics, Universidad Politécnica de Madrid, Avenida Juan de Herrera 6, E-28040 Madrid, Spain

(Received 29 July 2021; revised 29 January 2022; accepted 24 April 2022; published 2 June 2022)

Pathogen introduction in plant communities can cause serious impacts and biodiversity losses that may take a long time to manage and restore. Effective control of epidemic spreading in the wild is a problem of paramount importance because of its implications in conservation and potential economic losses. Understanding the mechanisms that hinder pathogen propagation is, therefore, crucial. Usual modelization approaches in epidemic spreading are based in compartmentalized models, without keeping track of pathogen concentrations during spreading. In this contribution we present and fully analyze a dynamical model for plant epidemic spreading based on pathogen abundances. The model, which is defined on top of network substrates, is amenable to a deep mathematical analysis in the absence of a limit in the amount of pathogen a plant can tolerate before dying. In the presence of such death threshold, we observe that the fraction of dead plants peaks at intermediate values of network connectivity, and mortality decreases for large average degrees. We discuss the implications of our results as mechanisms to halt infection propagation.

DOI: 10.1103/PhysRevE.105.064301

I. INTRODUCTION

Introductions of new plant pathogens into previously uncolonized areas is a major problem, since the feasible lack of defenses of the individuals in the area might cause fatal losses [1]. One example is sudden oak death, caused by the broad host range oomycete *Phytophthora ramorum*, which has caused devastating impacts on some North American and European forests [2]. In particular, it has killed millions of oak and tanoak in California since its first detection in 1995. Another noteworthy example of the impact of plant pathogen introduction is the massive economic damage caused by *Xylella fastidiosa*, a bacterium that affects 563 plant species from the Americas, Europe, the Middle East, and Asia. For example, an exhaustive study of the impact of this pathogen in olive trees can be found in Ref. [3].

During an epidemic outbreak, control decisions must be taken to lessen pathogen impact [4]. However, the restricted amount of time in which actions must be taken and the lack of information early in the epidemic often make the choice of action difficult [5,6] and the consequences can be extremely detrimental. The previously mentioned sudden oak death is a clear example: as pointed out by Cunniffe *et al.* [1], insufficient measures taken to eradicate the disease in California have led to a point where statewide action to even slow the spread of *Phytophthora ramorum* is no longer feasible; the pathogen has spread far enough that the only possible solution at present is local containment [1].

Thus, developing tools that allow us to better understand the behavior of new epidemics, and that help us predict what the outcome of different control measures might be, is a question of paramount importance. The main aim of this work is the analysis of the dynamics and stability, under different conditions, of a model for the spread of infections in wild plant populations, so that it can later be applied to real epidemics.

Most epidemiological models are based on a compartmentalization of individuals according to their disease status [7,8]. This is a notable simplification, for many details of the epidemic are neglected, for example, differences in response between individuals. The study of infection propagation on networks provides a way to include in the simulations different parameters related to the shape of the field in which the epidemic occurs, such as the spatial location of the individuals and the connectivity between different individuals. It also allows a better mechanistic understanding of the spread of the epidemic [9]. Traditionally, networks have been successfully used in human and animal epidemiology; however, not much work has been done for plant epidemics [10]. Here, we aim at modeling pathogen propagation infecting plant individuals on a spatial substrate. Plants have fixed spatial locations; hence contacts between individuals—due to neighboring relationships—are fixed as well (i.e., do not change over time), and such plant-to-plant spatial interaction mediated by the pathogen can be modeled by a static network of contacts between plant individuals. Even though plants do not change their location, plant-to-plant connectivity can vary if environmental conditions are taken into account: for example, intense wind conditions can help expand the effective number of contacts reachable from an infected plant. To properly model contagion in people or animal ensembles, one should unavoidably take into account a network of contacts whose structure varies *temporally* as individuals change their position.

Compartmentalized models like susceptible-infected-susceptible (SIS), susceptible-infected-removed (SIR), and further extensions of these generally do not track pathogen

[*]i.taguas@upm.es
[†]Complex Systems Group; Corresponding author: ja.capitan@upm.es
[‡]juancarlos.nuno@upm.es

concentrations over time. Instead, those models provide temporal variation of the fraction of individuals belonging to each class (infected, susceptible, recovered, etc.) during infection propagation over networked substrates [10,11]. Clustering individuals, e.g., plants or trees, into different classes makes infection dynamics more tractable. Instead, in this contribution we focus on pathogen densities across infected individuals and their variation over time, and we introduce and fully analyze a dynamical model for infection spreading defined by density-independent, per-capita fluxes of pathogen between individuals. In addition, we extract meaningful information when individuals are classified according to their response to infection. In particular, we assume that an individual is dead when pathogen abundance increases above a certain threshold. This means that the individual is effectively removed from the network, and does not contribute to the pathogen's propagation to other neighboring plants. Individuals can tolerate moderate epidemic charges (below the death threshold). It is precisely the presence of this threshold that enriches infection dynamics, which otherwise is amenable to analytical treatment in the absence of such a death threshold.

There is empirical evidence that individual plant death is related to pathogen load. Although the examples we used to motivate our study are protists infecting plants (*Phytophthora ramorum* or *Xylela fastidiosa*), the pathogens that spread over plant species range from viruses to fungi. In broad contexts (not only in the case of plant pathogens), it is commonly admitted that pathogen loads are correlated with the severity of active infections, which in turn leads to increased death odds. For example, there are many studies that correlate viral load with virulence and mortality (see, for instance, Refs. [12,13]). The same relationship has been reported for bacterial host-pathogen systems [14]. Experimental studies controlling the amount of *Phytophthora ramorum* infecting plant individuals show that pathogen load can be an indicator of the severity of the infection for a variety of host species [15]. Although surely there are exceptions to this rule, in general one can consider that increased pathogen loads lead to augmented harmful effects in the host, probably leading to frequent host mortality. The effect of uncontrolled pathogen propagation is particularly alarming in the case of the Californian sudden oak death caused by *Phytophthora ramorum* [16].

The effect of the substrate (mean field, network, lattice, etc.) on which epidemics take place has been extensively studied [17–22]. In these references a network's mean degree is usually fixed and epidemiological parameters controlling transmissivity are varied [23]. However, to the best of our knowledge, a comprehensive, quantitative assessment of the influence of network average connectivity on the fractions of healthy, infected, or dead individuals has been overlooked, surprisingly. Our main result is related to the number of dead individuals in the presence of a finite death threshold. We find that the fraction of dead plants peaks at intermediate network connectivity: for small connectivity, networks are basically disconnected and infection comes to a halt with a small number of dead plants. When networks are connected, increasing average degree favors channeling the pathogen across the network: the larger the mean connectivity, the smaller the fraction of dead individuals. Therefore, an effective mechanism to lessen the epidemiological impact in plant communities can be the facilitation of pathogen spreading over the network—for instance, by planting new pathogen hosts. Such a mechanism can be regarded as an alternative to obstructing or limiting propagation by isolating infected individuals.

II. EPIDEMIC SPREADING DYNAMICS

Our approach is based on a deterministic epidemic dynamics that unfolds on top of a network substrate, for which model parameters are random variables drawn from specified distributions. Across the network, each node represents an individual plant. Consider a plant pathogen infecting a network formed by n plants or trees belonging to the same species. Let x_i be the density of pathogen in plant individual i. When isolated (i.e., the pathogen is not transported among individuals), a logistic growth is assumed with rate $r > 0$ for pathogen abundance in each plant. This implicitly means that there is a carrying capacity K within each individual that limits pathogen abundance. The growth rate r has to be interpreted as a net rate $r = r_+ - r_-$ equal to the difference of the intrinsic birth rate minus mortality rate of the pathogen. Here, we take $r > 0$ because the pathogen has to grow (exponentially) in isolation in order for the infection to progress. Such exponential growth is attenuated by the carrying-capacity term when growth takes place within the host. This term effectively accounts for host immune systems in a way that pathogen growth is halted and the individual ends up with an asymptotic, constant amount of pathogen inside.

Plant individuals are accessible to host pathogen particles coming from adjacent plants. Pathogen transport is bidirectional: infected individuals can release pathogen particles to neighbors, and can also receive additional particles from neighboring plants. Such a flux of pathogen occurs among connected individuals i and j, for $i \neq j$. Networks are defined in a way such that two plants are connected if there is a nonzero probability of contagion between them. This probability depends on the dispersal ability of the pathogen, which is usually correlated to the distance between plant pairs. Therefore, we can assume that plants are disconnected if this probability is small; in other words, only pairs of individuals with probability of contagion above a threshold will be connected.

Consider a focal plant i. If there is a link in the network between i and j, the per-capita (per unit of pathogen abundance of the source individual) ingoing flux of pathogen from individual j to i is denoted as $a_{ij} > 0$, and the per-capita outgoing flux of pathogen from i to j as $b_{ji} > 0$. Flux direction is determined by the reverse order in indices, $a_{ij} = a_{i\leftarrow j}$ and $b_{ji} = b_{i\leftarrow j}$. Otherwise, if i and j are disconnected, then $a_{ij} = a_{ji} = 0$ as well as $b_{ij} = b_{ji} = 0$. In addition, we set $a_{ii} = b_{ii} = 0$ for $i = 1, \ldots, n$. Then, the amount of pathogen transported from j to i is equal to $a_{ij}x_j$, and the abundance transferred from i to j is equal to $b_{ji}x_i$. Refer to Fig. 1 for the interpretation of in- and outgoing pathogen fluxes.

Observe that, as defined, the nonzero entries of A and B define the network structure. If there is no link between i and j, then the corresponding entries in A and B are equal to zero, and vice versa. In other words, one can think of

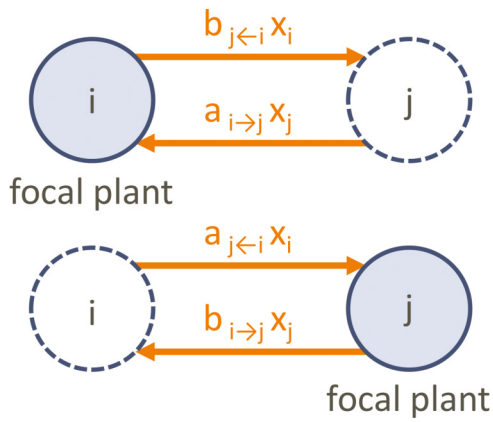

FIG. 1. Scheme for in- and outgoing fluxes of pathogen between nodes i and j, depending on which one is the focal plant.

$M = (m_{ij})$ as the adjacency matrix of a directed graph, representing the links that are actually realized in the network ($m_{ij} = m_{ji} = 1$ if there is a link between i and j, and zero otherwise). Then, one can define full random matrices A' and B' representing pathogen fluxes, and then set actual per-capita flux matrices $A = M \circ A'$ and $B = M \circ B'$, where $\circ$ stands for the Hadamard, component-wise matrix product. Therefore, nonzero elements of matrices A and B take into account realized links over the network.

Consequently, the coupled dynamics of pathogen concentrations are driven by a system of n coupled differential equations,

$$\frac{dx_i}{dt} = rx_i\left(1 - \frac{x_i}{K}\right) + \sum_{j=1}^{n} a_{ij}x_j - x_i\sum_{j=1}^{n} b_{ji}, \qquad (1)$$

for $i = 1, \ldots, n$. Observe that sums run over the set of neighbors of node i, given the restrictions imposed above for a_{ij} and b_{ij}. The connectivity of the plant community defines two matrices, $A = (a_{ij})$ and $B = (b_{ij})$. These per-capita in- and outgoing fluxes will be considered random variables. The parameters that define pathogen growth in isolation (r and K) will be varied throughout this study. Graphs are nondirected, meaning that if there is a flux of pathogen from individual j to individual i, there is also pathogen transfer from i to j. These fluxes, however, do not have to be balanced (this depends on the values of a_{ij} and b_{ji}).

If the fluxes of pathogen were to be *conserved across each link*, then $b_{ji} = a_{ji}$ and $b_{ij} = a_{ij}$ (see Fig. 1). In this case, $A = B$ and a single matrix would suffice to model this situation. In reality, losses or gains of pathogen occur: the ideal situation $A = B$, in which pathogen is conserved across any channel, is unrealistic. If there are pathogen losses at each link, a possible way to model that would be imposing $b_{ij} \geqslant a_{ij}$; i.e., the amount of pathogen that comes out from j to i, $b_{ij}x_j$, is greater than the amount received by i, $a_{ij}x_j$.

Observe that, if no restrictions are imposed to matrices A and B, the amount of pathogen transferred from a node is not necessarily equal to the overall pathogen amount that all its neighbors receive. In that case, the overall amount of pathogen in the plant community can increase (in the presence of an external source) or decrease (if there are additional mechanisms that channel pathogen particles out of the system). Otherwise, the overall amount of pathogen that comes out from any node i can be distributed among its neighbors. If the amount that comes out from i *equals* the overall quantity received by *all* its neighbors, then there are no losses of pathogen during infection spreading and the transport process is *conservative*. This condition can be easily formulated, because the total amount of pathogen that comes out from i is equal to $x_i\sum_j b_{ji}$, according to previous definitions. On the other hand, a neighbor j receives from node i an amount of pathogen equal to $a_{ji}x_i$, so the total quantity received by neighbors is $x_i\sum_j a_{ji}$, just by summing over the neighbors of node i. Thus, the conditions for no pathogen losses during transport are

$$\sum_{j=1}^{n} a_{ji} = \sum_{j=1}^{n} b_{ji} \qquad (2)$$

for $i = 1, \ldots, n$. If these conditions are satisfied, we say that the transport process is conservative, because there are no losses of pathogen during transfers between individuals. This scenario conserves the overall pathogen transmitted through links over the network, a more general situation that does not necessarily force that fluxes are exactly the same across each channel (as for the $A = B$ case). Observe that the only restriction imposed to matrices A and B is that their row sums are conserved. This case, however, can be modeled using only a single matrix, because if one inserts condition (2) into Eq. (1), the dynamics only depends on matrix A:

$$\frac{dx_i}{dt} = rx_i\left(1 - \frac{x_i}{K}\right) + \sum_{j=1}^{n} a_{ij}x_j - x_i\sum_{j=1}^{n} a_{ji}. \qquad (3)$$

Although at any time there are no gains or losses of pathogen during transport processes in the conservative case, the overall amount of pathogen in the system is not constant over time because its infectious particles reproduce within hosts. This can be deduced from Eq. (3) by summing all the equations. Then one gets

$$\frac{d}{dt}\sum_{i=1}^{n} x_i = r\sum_{i=1}^{n} x_i\left(1 - \frac{x_i}{K}\right), \qquad (4)$$

because in a conservative situation internal fluxes are globally balanced across the network [i.e., the two last terms in Eq. (3) cancel when summing over i]. The right-hand side of Eq. (4) is not initially equal to zero, so the overall amount of pathogen can increase or decrease until reaching equilibrium. Due to pathogen reproduction inside each individual, the total pathogen abundance in the system can increase from its level at time $t = 0$ until reaching the steady state.

Unless the contrary is specified, we will not impose any restriction on matrices A and B, for the sake of generality. This is the most general setup, which indeed can be fully studied, both analytically and numerically. Other situations that conserve fluxes across links, or globally across each node's neighbors, are basically particular cases of this general formulation.

For our model, we have defined three plant states (node compartments) depending on the host's epidemic concentrations x_i: individuals can be healthy (pathogen concentration

equal to zero), infected (pathogen abundance above zero and below a certain death threshold δ), or dead (pathogen concentration above the death threshold). Therefore, the death threshold can be interpreted as the maximum pathogen amount an individual can hold to remain alive. When the death threshold is exceeded, the plant dies and disappears from the network. At this moment, it is assumed that the complete concentration of pathogen vanishes. Thus, plant death modifies immediately network topology as well as pathogen dynamics.

III. QUALITATIVE ANALYSIS WITHOUT MORTALITY

Before reporting simulation results obtained for different network architectures, here we briefly summarize the qualitative analysis of Eq. (1) in the absence of plant mortality (i.e, in the limit $\delta \to \infty$) in two scenarios besides the conservative case defined above:

(i) A *per-capita flux balance* condition is satisfied. In this case, the overall ingoing per-capita flux of a node is balanced by the overall outgoing per-capita flux associated to the same node. This condition reduces, for an arbitrary node i, to

$$\sum_{j=1}^{n} a_{ij} = \sum_{j=1}^{n} b_{ji}, \quad i = 1, \ldots, n. \tag{5}$$

Notice the difference between Eq. (2) and Eq. (5).

(ii) *No restriction* is imposed in per-capita flux matrices A and B.

We do not make here explicit assumptions about network structure, which is implicitly contained in matrices A and B.

Case (i) has been contemplated because it is amenable to a complete stability analysis. The proofs of the following results are provided in Appendix A. It can be shown that, if the network is connected, our model always exhibits two equilibrium points: $\boldsymbol{x}^\star = \mathbf{0} := (0, \ldots, 0)$ and $\boldsymbol{x}^\star = K\mathbf{1} = (K, \ldots, K)$, for $\mathbf{1} := (1, \ldots, 1)$. Moreover, the first equilibrium point, which corresponds to pathogen clearance, is unstable. The second one, associated to a full infection situation (all individuals are infected), is globally asymptotically stable, though. Therefore, in the absence of a death threshold, it is expected that all individuals within a connected component of the network will end up infected.

The stability analysis yields comparable results for the general case of arbitrary (unrestricted) per-capita pathogen fluxes between individuals. In case (ii) it is not possible to compute explicit expressions for the equilibrium points. However, if matrices A and B are random, it is *almost sure* that, for connected networks (i.e., there is a single giant component), the only equilibria observed for Eq. (1) correspond to either pathogen clearance, $\boldsymbol{x}^\star = \mathbf{0}$, or full infection, $\boldsymbol{x}^\star = (x_i^\star)$, with $x_i^\star > 0$ for every node, $x_i^\star$ not necessarily equal. Two situations can occur, depending on network connectivity: (a) a single equilibrium point emerges, $\boldsymbol{x}^\star = \mathbf{0}$, which is stable; and (b) both equilibrium points arise, one associated to pathogen clearance being unstable, and one relative to pathogen full infection being stable. Note that the full infection equilibrium emerges and is stable when the pathogen clearance one becomes unstable.

Although it is difficult to analytically show that the full infection equilibrium exists [case (b)], we numerically found that this is precisely the most probable case, especially for sparse random networks above (but close to) the percolation threshold. For larger network average connectivity, case (a) becomes more frequent (not dominant, though), and model realizations in which infection disappears can be observed in simulations (see Fig. 8 in Appendix B). Observe that the qualitative analysis summarized here for the general case (ii) applies as well for the conservative scenario defined by Eq. (2).

Therefore, in the absence of a death threshold, it is expected that the pathogen spreads throughout the entire network with high probability if the network is connected. Considering a maximum value in pathogen concentration above which an individual is regarded as dead, however, makes it very difficult to predict which plant is to become extinct and which one will survive (although infected) starting from arbitrary initial conditions, unless one is resorting to the numerical integration of the system of differential equations.

IV. PLANT MORTALITY AND NETWORK DYNAMICS

In the presence of a (finite) death threshold δ, every infected plant whose epidemic charge exceeds the mortality threshold will die. When mortality occurs, automatically, the corresponding node is disconnected from the network, as well as the associated in- and outgoing fluxes (which are set equal to zero). Importantly, network topology is temporally coupled with the infection propagation dynamics. Initial networks can change their size and topological properties due to the demise of some of the individuals during the epidemic. As we will show below, the introduction of a mortality threshold in pathogen concentrations changes drastically the scenario portrayed in the qualitative analysis of the model without such an upper bound on tolerable epidemic charges.

We use two different network architectures: random graphs drawn from the Erdős-Rényi (ER) model [24], and random geometric (RG) [25] models. In the absence of any particular knowledge about plant locations, we assume that links are drawn at random. Specifically, it is assumed that there is a uniform probability of linking two nodes, as defined by the classical ER model. The outcome of the ER model is a graph $G(n, p)$ in which n is the number of nodes and p is the probability that two nodes are linked; i.e., links are placed randomly and independently between distinct pairs of nodes with probability p.

In situations governed by short-range pathogen dispersal, however, the probability of contagion is related to distance. As a consequence, it is natural to assume that closer nodes have a larger probability of being connected. This assumption is applied to build RG networks. A random geometric network is the simplest kind of spatial network. Nodes are embedded in a metric space, and two nodes could be connected if and only if the Euclidean distance between them is in a given range—for instance, smaller than a certain neighborhood radius, R [26]. Therefore, two nodes that are within the same area of influence are randomly connected as in the ER model. Nodes that are out of this area of influence are not connected.

Nodes in our RG networks are drawn uniformly on the unit square $[0, 1] \times [0, 1]$. We assume that connection probability explicitly depends on the distance between nodes. We used

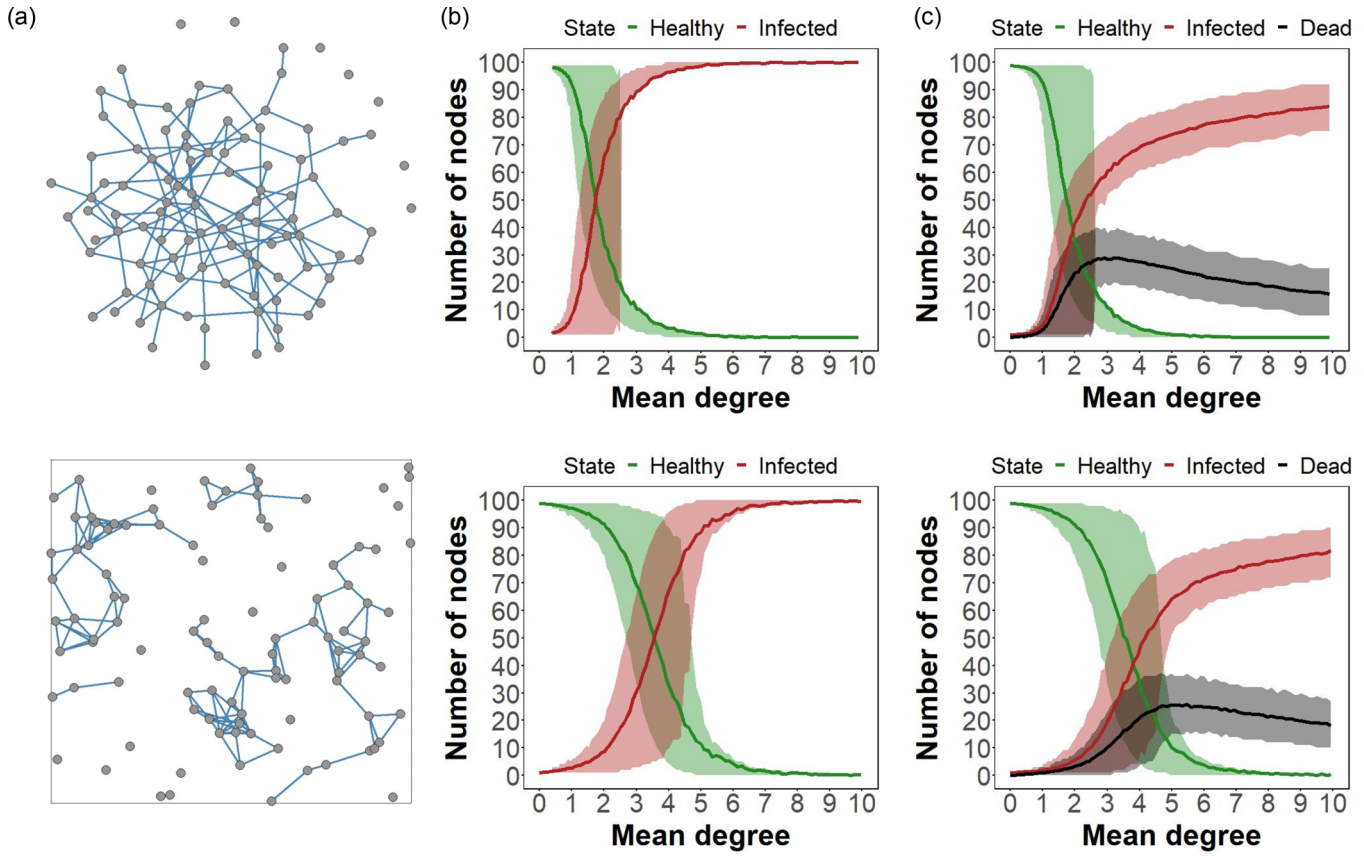

FIG. 2. Number of healthy, infected, and dead plants. Upper (lower) panels correspond to ER (RG) graphs. (a) Top: Example of an ER network drawn from $G(100, 0.03)$ with a connection probability $p = 0.03$. Bottom: Example of a RG network with $n = 100$, $R = 0.15$, and $p = 1$ on the unit square. (b) Number of healthy (green) and infected (red) nodes in simulations carried out without a death threshold ($\delta \to \infty$) as functions of mean degrees of networks. (c)Number of healthy (green), infected (red), and dead (black) nodes in the presence of the death threshold ($\delta = 0.9K$) as functions of initial network mean degree. In (b) and (c), the horizontal axis is calculated as the expected mean degree of the initial network, i.e., the mean averaged degree over realized networks, which is equal to $\mathrm{E}[k] = (n-1)p$ for ER sampled graphs. The shaded areas are defined by the 10th and 90th percentiles. Here, $r = 0.5$ and $K = 1$. A maximum in the number of dead nodes arises in both cases; in ER networks this happens at a mean degree of around 3, and in RG networks at a mean degree of around 5. Each panel was calculated by averaging over 1200 initial conditions, networks, and matrix realizations.

the following continuous function:

$$p_{ij} = \begin{cases} \left[1 - \left(\frac{d_{ij}}{R}\right)^2\right]p, & d_{ij} \leqslant R \\ 0, & d_{ij} > R, \end{cases} \tag{6}$$

which means that when the distance between i and j is smaller than R, there is a nonzero probability of connection dependent on that distance (the closer the nodes are, the greater the chance they are connected). The parameter $0 < p \leqslant 1$ is interpreted as follows. When the distance between pairs of nodes is above the radius, they are never connected. In the limit $R \to \infty$, the distance cutoff R is removed and nodes are connected with probability p; i.e., two nodes are linked at random with probability p, as in the ER model. Therefore, RG networks yield ER graphs in the limit of large distance cutoffs. Throughout this work we present results for RG networks with $p = 1$ (we choose RG networks to be as far away as possible from ER ones). Samples of the RG network model with size n and radius R will be denoted by $G(n, R)$. Our results are not dependent of the specific functional form (quadratic, in this case) of connection probability given by Eq. (6).

In simulations, the entries of matrices A and B were independently and randomly drawn from a uniform distribution $U(0, 1)$. The dynamical model (1) was integrated numerically until convergence to an equilibrium steady state. As the dynamics unfolds, a number of nodes can go extinct if their concentration is above the threshold δ, and this process continues until no concentration exceeds the threshold across the system. Nodes that remain alive will reach the corresponding equilibrium state.

Simulations were conducted using networks formed by 100 nodes. Unless the contrary is specified, we used a growth rate value $r = 0.5$ and a carrying capacity value $K = 1$. As for the death threshold, we set it as $\delta = 0.9K$. As the initial condition, we picked up randomly a node as infected with an initial pathogen load randomly drawn from the uniform distribution $U(0, \delta)$.

V. SIMULATION RESULTS

In Fig. 2 we report results for the infection process operating on networks with increasing connectivity. Figure 2(a)

shows two samples of ER and RG network models with about $L = 150$ links overall. Clearly, for that number of links, ER graphs are closer to the percolation threshold—estimated as $p_c \approx 1/n$ [27]—which is evidenced by a large connected component. For $L \approx 150$, RG networks are comprised of more isolated nodes and smaller components. The radius above which a giant component arises in RG graphs is estimated as $R_c \approx \sqrt{\log n/(n\pi)}$ [26]. Figure 2(b) shows how the numbers of healthy and infected nodes vary as functions of the mean degree when plant mortality is not considered (i.e., when the death threshold goes to infinity), whereas Fig. 2(c) reports the same results for the number of healthy, infected, and dead nodes versus mean degree in the presence of a finite death threshold. We observe in both panels that ER and RG curves are similar, but displaced to the right for RG graphs.

As shown in Appendix B, when the network is connected, we expect that every node is infected (at least in the range of average degrees reported in Fig. 2) in the absence of plant mortality. For mean degrees well above the percolation threshold, this is what we observe in Fig. 2(b). On the other hand, if the network is not connected, it is apparent that pathogen spreading will not progress in those components that were not initially infected. It is only close to the percolation threshold of these networks that the curve of healthy individuals starts declining. This is consistent with the expected degree $\mathrm{E}[k]$ at the percolation threshold (k_i stands for the degree of node i). For an ER graph $G(n, p)$, $\mathrm{E}[k] \approx (n-1)p$ [27], which is of the order of unity at $p = p_c \approx 1/n$. For a RG graph $G(n, R)$, $\mathrm{E}[k] \approx n\pi R^2$ [26], which reduces to $\mathrm{E}[k] \approx \log n$ at $R = R_c \approx \sqrt{\log n/(n\pi)}$. Therefore, for $n = 100$ we expect the transition at mean degrees about 4.6 for RG networks and about 1 for ER networks. The decline of the number of healthy plants in both cases is observed at mean degrees consistent with these estimations (Fig. 2). This analysis suggests that network connectivity is an important driver of the overall outcome of infection spreading.

Plant mortality arises for finite values of the death threshold δ. According to Fig. 2, the number of dead nodes peaks at a mean degree value around $\mathrm{E}[k] \approx 3$ for ER graphs and around $\mathrm{E}[k] \approx 5$ for RG networks. We observe this maximum in mortality independently of the values taken by the growth rate, carrying capacity, and death threshold. These parameter values do affect the location of the maximum, though. The same phenomenon occurs in the conservative scenario for ER graphs (see Fig. 3). Conservation of transported pathogen in RG networks yields similar results.

These maxima in the number of dead plants seem counterintuitive. One might expect that the higher the connectivity of the network, the lower the number of dead plants, because the pathogen should be effectively distributed among a larger number of neighbors, leading to less plants above the death threshold. However, there is an intermediate network connectivity with the highest death rate. To test whether these maxima were due to the networks being disconnected for lower mean degrees, we repeated these simulations for small-world networks (Appendix C). We used the Watts-Strogatz (WS) small-world model [28], which introduces link rewiring of regular networks yielding graphs formed by a single connected component. In this case, we do not observe a maximum in the number of dead nodes for any mean degree;

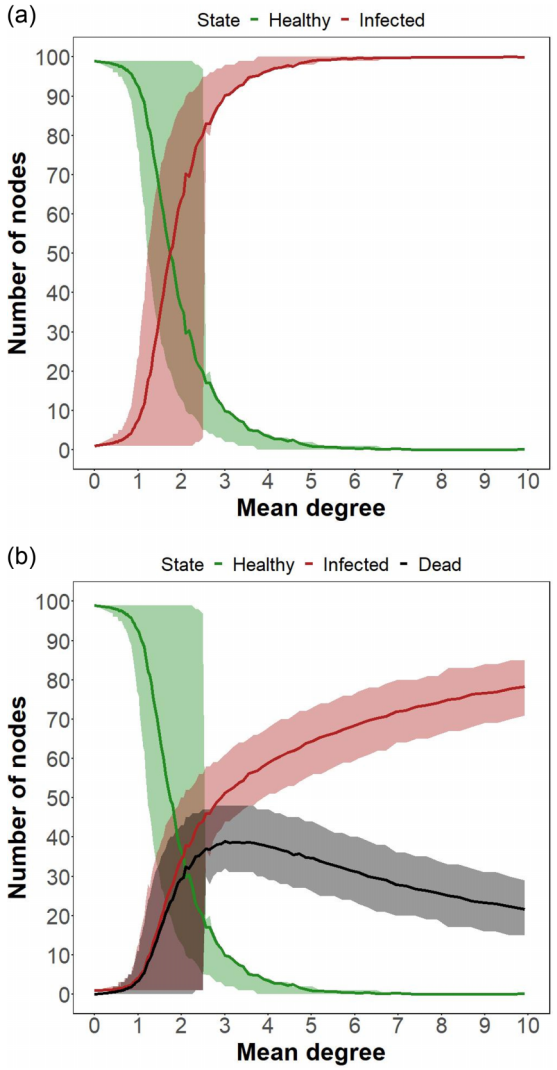

FIG. 3. Conservative model. Here we reproduce Figs. 2(b) and 2(c) for the dependence of the number of individuals within compartments (healthy, infected, or dead) with ER network mean degree, when conservation of pathogen [Eq. (2)] is imposed in the dynamics.

plant mortality decreases monotonically as the mean degree increases. The reason is that, in small-world networks, no matter how low the mean degree is, the network is always connected. Infection can spread throughout the network, and for larger degrees the epidemic load can be channeled out through a higher number of ways, thus reducing the asymptotic pathogen abundance of each node and, consequently, not exceeding the death threshold.

Once the network is connected, or has just a few isolated nodes, if nodes are connected on average with a higher number of neighbors, pathogen particles can be transported more efficiently between plants and the overall pathogen charge is distributed across the network, leading to more individuals with concentrations below the threshold δ. It is difficult for the pathogen to reach the death threshold in a given individual, for there are many outgoing fluxes to many other individuals, swiftly distributing the pathogen.

This hypothesis can be confirmed in Figs. 4 and 5, which show the relationship between network connectivity and

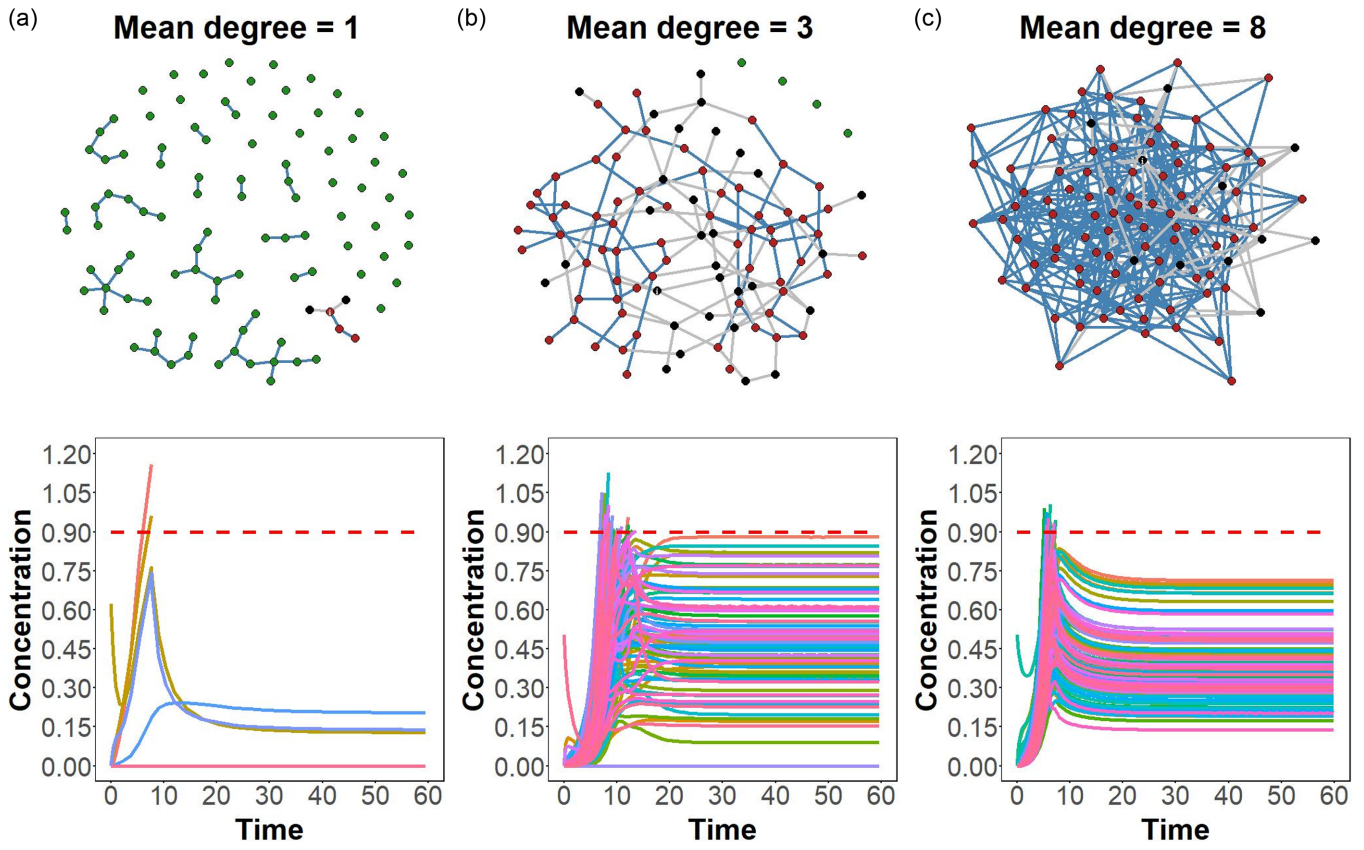

FIG. 4. Random network connectivity and pathogen temporal dynamics. ER networks with mean degrees (a) E[k] = 1, (b) E[k] = 3, and (c) E[k] = 8. Upper panels depict the end state of sampled networks after the disease has spread. Healthy (green), infected (red), and dead (black) nodes are represented. Blue links remain after reaching the end state (links connecting dead nodes are colored in grey). In all cases, in the initial state of the network only one node is infected. As for the end state, in (a) the fractions (H, I, D) of healthy, infected, and dead plants are (H, I, D) = (0.95, 0.03, 0.02). In (b) and (c) we end up with fractions (H, I, D) = (0.04, 0.66, 0.3) and (H, I, D) = (0, 0.89, 0.11), respectively. Lower panels show the temporal variation of each node's pathogen concentration. The dashed line indicates the death threshold value.

pathogen temporal dynamics. We have considered ER graphs with three connectivity values: (i) below the maximum in the number of death nodes (E[k] = 1), (ii) at the maximum (E[k] = 3), and (iii) well above the maximum (E[k] = 8). For these cases, we have obtained (Fig. 5) the distributions of the size of the connected component which the initially infected node belongs to, as well as the size distribution of the largest connected component that ends up fully infected.

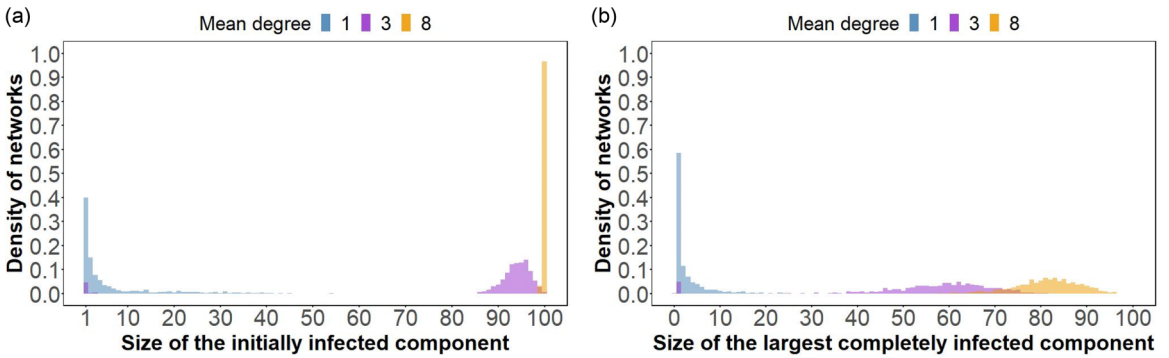

FIG. 5. Size of the largest infected components. Colors correspond to those of Figs. 4(a)–4(c), i.e., ER networks with mean degrees E[k] = 1 (blue), E[k] = 3 (purple), and E[k] = 8 (orange). (a) Distribution of the size of the connected component which the initially infected node belongs to (1200 realizations for each mean degree). (b) Size distribution of the largest completely infected component at the end of simulations, showing that networks break up once the dynamics unfolds. The location of the distributions, which correlates to existence of a giant component, is put into correspondence with temporal dynamics, leading to a small fraction of infections and deaths (blue), a maximum number of dead nodes (purple), and the distribution of pathogen loads across the network, leading to fewer deaths (orange).

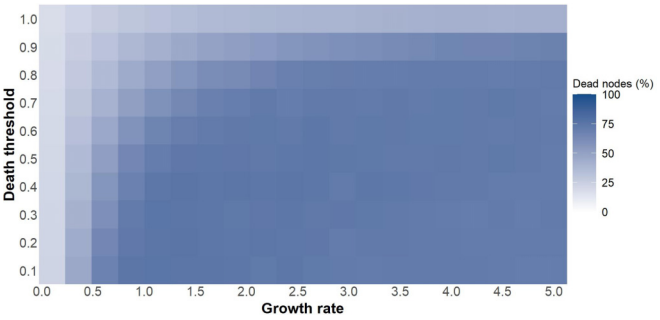

FIG. 6. Fraction of dead nodes for variable death threshold and growth rate. For fixed growth rates, mortality decreases as the death threshold increases. When the death threshold is constant, the fraction of dead nodes augments for increasing growth rates until reaching a rather constant plateau. This can occur sharply or smoothly depending on the values of the death threshold.

Note that, according to our analytical results, once the process has relaxed and every survivor has abundance below the death threshold in an infected component, we expect that the full component will remain infected until reaching the steady state (this is illustrated in Fig. 4, lower panels). As the initially infected node is in a larger component, we observe that the temporal dynamics leads to increasing death events. However, for mean degrees leading to fully connected networks, the average pathogen load per individual is smaller, because pathogen particles are more evenly distributed due to the network's higher connectivity. Indeed, for low mean degree ($\mathrm{E}[k] = 1$), the size of the initially infected component is small, and the network is initially broken into pieces, so infection is able to progress only within the initial group and the expected number of deaths is low. For intermediate mean degree ($\mathrm{E}[k] = 3$), the initially infected component is large, but the epidemic process breaks the network and, as a consequence, the size of the largest component that ends up fully infected lowers. For large connectivity ($\mathrm{E}[k] = 8$), almost every plant belongs to the initially infected component. Such connectivity allows for an effective distribution of the overall pathogen load across nodes, many of them remaining below the death threshold. The initial component size in this case decreases because dead nodes are removed from the initial cluster. Hence, the maxima in mortality are explained: once a network is connected, higher connectivity implies lower mortality rates, due to the distribution of pathogen over a larger number of nodes as the epidemic spreads.

To see how remaining model parameters affect plant mortality, we set the carrying capacity to $K = 1$ and varied the death threshold ($\delta \in [0.1, 1]$) and the growth rate ($r \in [0.1, 5]$). The percentage of dead nodes as function of the growth rate and the death threshold are shown in the heat map represented in Fig. 6.

For fixed values of the growth rate, the number of dead nodes decreases as the death threshold increases. This is an intuitive result, since a higher death threshold implies a lesser fraction of killed plants. When the death threshold is equal to the carrying capacity ($K = 1$), the number of death nodes for any growth rate is significantly lower than with any other death threshold.

If the death threshold is fixed, mortality increases as the growth rate augments until reaching an approximately constant value that depends on δ. Such an increase can be sharper (smoother) for smaller (larger) values of δ. This is due to the fact that when the ratio between growth rate and death threshold is large enough, nodes die too quickly, disconnecting the network and hindering the spread of the disease. In summary, mortality becomes more pronounced for large pathogen growth rates and small values of the maximum pathogen concentration that an individual can tolerate.

We have tested the robustness of our main result, i.e., the emergence of a peak in mortality as the network's average connectivity increases, in three scenarios: (i) when each individual plant has a characteristic death threshold δ_i (instead of the case of constant δ studied above), (ii) when per-capita fluxes are drawn from distributions with different means, and (iii) when the remaining concentration of pathogen after an individual's death is not neglected and can infect other neighbors. We summarize the results of these robustness tests in Appendix D. Our results remain robust when these modifications are taken into account.

VI. DISCUSSION

In this work we have presented and fully analyzed a mathematical model of pest dynamics, acting on plant communities, that keeps track of pathogen concentration across individuals over time. Our approach considers a death threshold, above which plants die. We have shown that the introduction of this threshold modifies substantially the infection dynamics. Contrary to the case where no threshold exists, individual deaths modify network topology over time, because individuals whose pathogenic charge exceeds the threshold are no longer connected. A counterintuitive result appears: networks with higher connectivity yield a larger fraction of individuals that survive. We can explain the phenomenon using a channeled flux analog: if the percolation threshold has been crossed over and there exists a giant component, for equal pathogen growth rate and death threshold values, a higher connectivity enables a better drainage of pathogen particles across the network, which precludes a larger number of individuals from reaching their death threshold. What remains is a network formed by infected individuals that are resistant to the pathogen in the long run.

Phytophthora ramorum is a pathogen mainly transmitted by air. However, many plant pathogens are transmitted by insects. Our model could be effectively modified to consider vectors transmitting the infection. We decided not to consider an explicit species mediating the infection to keep the model as simple as possible. In any case, the overall pathogen transport in our model is taken into account by matrices A and B. Then, the average effect due to the explicit consideration of a new species mediating infection propagation could be subsumed into the transport mechanisms represented by both matrices. Given that there are at most $2n(n-1)$ coefficients in both matrices, for large n there are free parameters enough to fit any mechanism of transmission mediated by a number of vectors carrying the pathogen themselves between individuals.

As for the robustness of our main result, we have used different network structures (ER and RG) and implemented different conditions relative to potential pathogen losses or gains during transportation (balanced fluxes, conservative approach, and unrestricted fluxes). The maximum in mortality arises as long as the network changes from being disconnected to connected—we do not find the maximum in model networks that have no percolation transition, such as in the WS model. Therefore, the incidence of the epidemic across a population is determined by network structure. As far as we know, fatality rates in plant epidemics have not been previously connected with network average connectivity. In addition, we varied model parameters (pathogen growth rate and death threshold) and—not surprisingly—we found that restrictive death thresholds and highly reproductive pathogens yield the highest fractions of dead nodes.

We have also tested the robustness of this result using idiosyncratic (individual-dependent) values of the death threshold as well as different mean values for transport coefficients, and tracked how the remaining pathogen (after an individual death) diffuses across the system. Throughout this contribution we used random values for per-capita fluxes of pathogen between individuals. Random matrices represent an appropriate framework to model large systems for which it is difficult to infer actual interaction strengths, as well as to provide consistent predictions about diversity and stability [29,30].

Except for the position of the maximum, which in RG networks takes place at larger mean degrees, we did not find remarkable differences with the dynamics on ER networks regarding fatality and infectivity. The RG model is more realistic because nodes are embedded in a plane, as plants in communities, and neighboring relations between them are better defined depending on distance. However, these features are not determinant when it comes to quantifying mortality rates during epidemic spreading.

Temporal dynamics shown in Fig. 4 illustrate the appearance of the maximum in mortality. When a giant component starts forming, most of the nodes get infected, resulting in the propagation of the disease. However, since the mean degree is not very high, it takes longer to reach all the nodes [see Fig. 4(b), lower panel]. Pathogen grows inside infected hosts and take longer to spread, so a higher number of plants can effectively cross over the death threshold, increasing mortality numbers. Larger connectivity (above the maximum), however, implies that dead nodes reach the threshold in a more synchronous way [Fig. 4(c), lower panel]. Because connectivity is large, the network remains connected and the qualitative analysis provided in Sec. III ensures that a full infection equilibrium state (for the plants that remain alive) will be reached with high probability.

Our work has broader implications beyond plant epidemic propagation on spatial substrates. Equation (1) can be interpreted as a metapopulation model on top of a network substrate connecting patches, in which individual plants are the counterpart of patches and pathogen particles are equivalent to a population's individuals moving between patches. It is important to remark that the network of patches is not new to this contribution [31]. Our results directly apply to situations where the occupancy of each patch is to be limited by a maximum number of individuals and, being fully occupied, the patch becomes disconnected from the network. Then the fraction of "fully occupied patches" should peak as the average degree increases. Other than that, we provide a fully detailed mathematical analysis of the metapopulation model when random transport coefficients are considered, so the qualitative analysis we carried out can also be useful in the context of ecological metapopulation models.

There are many examples of plant and crop infection situations that are mediated by diffusive processes. For example, recently it has been shown that plant pathogen spores spreading fungal diseases can be dispersed even in the complete absence of rain or strong winds [32]. More importantly, short-distance aerial and rain-splash dispersal has been reported for *Phytophthora ramorum* [33]. Surely there are many more examples of plant pathogen dispersal in which short-distance transport mechanisms drive disease propagation, with a well-defined distance cutoff. For these cases, one has to resort to short-range dispersal mechanisms to see how infection progresses, and our approach based on RG networks can be a good starting point. Even in the case that long-range dispersal drives epidemic spreading, any modeling attempt should include a combination of local infections and long-range jumps. One can separate both processes and use our model as well: consider an infected region where a long-range jump to an uncolonized area takes place. Then spreading starts in that region with a single infected plant (as in our approach) far away from the originally infected individuals. This infective propagule can cause local dispersion dynamics in the neighborhood of the initially infected plant, which could be modeled as a separate system from the original focus.

Countless studies based on compartmentalized models have focused on finding thresholds in effective spreading rates above which infection progresses and reaches every node (see Ref. [34] and references therein). For SIS models on heterogeneous networks, the mean field epidemic threshold is known to be equal to $\langle k\rangle/\langle k^2\rangle$, where $\langle\cdot\rangle$ stands for an average value [35]. Such thresholds do not arise in our model because pathogen can be effectively spread across the giant component. For that reason, our results have to be recast in terms of how pathogen distributes depending on network connectivity.

It is important to stress that our model tracks pathogen dynamics on each individual plant, without using aggregated variables within compartments; i.e., we do not model the fractions of susceptible (healthy), infected, and removed (dead) plants as functions of time, as standard SIR *effective* models do. Our *microscopic* dynamics describes the concentration $x_i(t)$ of pathogen over time, which is the one that truly takes place during infection propagation, and then (thanks to the introduction of the death threshold δ) we categorize each plant into three classes (healthy, infected, or dead) depending on pathogen concentrations. Our approach is bottom up, trying to infer the fractions of individuals within compartments from a microscopic dynamics, without modeling those fractions themselves. In principle, there is no certainty that an effective model, similar to standard SIR dynamics, would reproduce the microscopic dynamics, so it is fair to question whether these two temporal dynamics can be comparable or not. In Appendix E, we provide a detailed comparison of the microscopic dynamics, aggregated into classes, compared to two

formulations of the SIR model, which both fail to capture quantitatively the occupancies of each class.

Our work helps infer effective mechanisms that can hinder, or even halt, epidemic spreading across plant communities. For communities in which plants are scattered, it is dificult for the infection to propagate among disconnected network components, at least, in short time scales. Obviously, long-range dispersal can occur and uncolonized components can become infected in the long run. However, in diverse communities, packed individuals are accessible to pathogen transfers. Probably local containment to restrict propagation is not effective in highly connected systems. Our results suggest that a plausible mechanism to alleviate pathogen charges across communities is precisely increasing the connectivity by planting new individuals. Then a "dilution effect" can take place [36], because a higher number of susceptible individuals will reduce the disease burden in a focal plant because other susceptible neighbors will share the load of pathogens.

For example, *Viburnum acerifolium* [37] is a shrub that coexists with the Californian oak, and both are infected by *Phytophthora ramorum* [38]. Shrub individuals grow fast compared to oaks and could alleviate oak pathogen levels shortly after being planted, if oak epidemic spreading could be effectively approximated by the mechanisms that drive our model dynamics. New individuals will "drain" pathogen particles from the species to be protected. Although infection may pervade the whole system, larger connectivity values will lower pathogen loads, which will be more tolerable for plants targeted by conservation strategies. Thanks to pathogen reduction measures like this, infected individuals, ultimately, will survive until recovery protocols are available.

Obviously, for this strategy to be effective, shrubs should be more resistant to the pathogen; otherwise, they could act as superspreaders and increase pathogen loads in oaks. This could be effectively achieved if $K_{\text{shrub}} \ll K_{\text{oak}}$, so that in isolation the pathogen reaches a lower saturation level in shrubs than in oaks. A similar way to obtain the same outcome is choosing a shrub species such that the pathogen grows slower than in oaks, i.e., $r_{\text{shrub}} \ll r_{\text{oak}}$. Although our model should incorporate a second species to properly draw this conclusion, current evidence from our work suggests such a possibility and leaves open its viability to be checked in further refinements incorporating two separate species.

APPENDIX A: STABILITY RESULTS FOR PER-CAPITA FLUX BALANCE

In this section we provide proofs for the results stated in Sec. III for the per-capita flux balance dynamics. We first calculate the attractors of the dynamics.

Theorem 1. Assume that the graph M associated to matrices A and B is connected, and that per-capita fluxes are balanced; i.e., Eq. (5) holds. Then the only equilibrium points of Eq. (1) are either $x_1^\star = \cdots = x_n^\star = 0$ or $x_1^\star = \cdots = x_n^\star = K$.

Proof. We want to solve the nonlinear system of equations

$$r x_i^\star \left(1 - \frac{x_i^\star}{K}\right) + \sum_{j=1}^{n} a_{ij} x_j^\star - x_i^\star \sum_{j=1}^{n} b_{ji} = 0, \tag{A1}$$

$i = 1, \ldots, n$. Completing squares, we can write the system as

$$\left(x_i^\star - \frac{K}{2}\right)^2 = \frac{K^2}{4} + \frac{K}{r}\left(\sum_{j=1}^{n} a_{ij} x_j^\star - x_i^\star \sum_{j=1}^{n} b_{ji}\right) = 0. \tag{A2}$$

Define the new variables $y_i := x_i^\star - \frac{K}{2}$. With these new variables, the system reduces to

$$y_i^2 = \frac{K^2}{4} + \frac{K}{r}\left(\sum_{j=1}^{n} a_{ij} y_j - y_i \sum_{j=1}^{n} b_{ji}\right) = 0. \tag{A3}$$

Without loss of generality, we can sort the entries of vector $\boldsymbol{y}$ by relabeling equations and write $-\frac{K}{2} \leqslant y_1 \leqslant y_2 \leqslant \cdots \leqslant y_n$. Then Eq. (A3) for $i = 1$ yields

$$\begin{aligned} y_1^2 &= \frac{K^2}{4} + \frac{K}{r}\left(\sum_{j=1}^{n} a_{1j} y_j - y_1 \sum_{j=1}^{n} b_{j1}\right) \\ &\geqslant \frac{K^2}{4} + \frac{K}{r}\left(\sum_{j=1}^{n} a_{1j} - \sum_{j=1}^{n} b_{j1}\right) y_1 = \frac{K^2}{4}, \end{aligned} \tag{A4}$$

where we have used the assumption that $y_j \geqslant y_1$ for $j = 2, \ldots, n$ and the equality of in- and outgoing fluxes [cf. Eq. (5)]. From Eq. (A4) we have that either $y_1 = -\frac{K}{2}$ or $y_1 \geqslant \frac{K}{2}$. We consider these two cases separately.

(a) Let $y_1 = -\frac{K}{2}$. Since the network is connected, a shortest path over the network exists such that node 1 is connected to node n, either directly through an existing link or by a finite series of steps using intermediate nodes. Let $\{i_1, i_2, \ldots, i_s\}$ denote the index sequence for the path connecting node 1 and node n. Then $a_{1,i_1} > 0$ and assume that $y_{i_1} > -\frac{K}{2}$. Because $\sum_j a_{1j} y_j > -\frac{K}{2} \sum_j a_{1j}$ (notice that the strict inequality is due to the variables being sorted, which implies that $y_k > -\frac{K}{2}$ for $k > i_1$), Eq. (A3) for $i = 1$ reduces to

$$0 = \sum_{j=1}^{n} a_{1j} y_j + \frac{K}{2} \sum_{j=1}^{n} b_{j1} > \frac{K}{2}\left(-\sum_{j=1}^{n} a_{1j} + \sum_{j=1}^{n} b_{j1}\right) = 0, \tag{A5}$$

which is obviously a contradiction. Therefore, $y_{i_1} = -\frac{K}{2}$, which implies that $y_1 = \cdots = y_{i_1} = -\frac{K}{2}$. This argument can be iterated until reaching node n. Now consider node i_1, which in the path is connected to i_2. If $i_2 > i_1$ then we apply the same argument [using that $a_{i_1,i_2} > 0$ in Eq. (A3) particularized for $i = i_1$] to prove that $y_1 = \cdots = y_{i_2} = -\frac{K}{2}$. If $i_2 < i_1$, then we iterate the procedure for the following node in the sequence, i_3. At the end of the path we will reach node i_s, connected to the end point at node n. Then Eq. (A3) for $i = i_s$, together with the fact that $a_{i_s,n} > 0$, implies that $y_1 = y_2 = \cdots = y_n = -\frac{K}{2}$ in this case. This solution reduces to $x_1^\star = \cdots = x_n^\star = 0$.

(b) Assume now that $y_1 \geqslant \frac{K}{2}$. Now particularize Eq. (A3) for $i = n$. Using that $y_j \leqslant y_n$, we can find the following upper bound for y_n^2:

$$\begin{aligned} y_n^2 &= \frac{K^2}{4} + \frac{K}{r}\left(\sum_{j=1}^{n} a_{nj} y_j - y_n \sum_{j=1}^{n} b_{jn}\right) \\ &\leqslant \frac{K^2}{4} + \frac{K}{r}\left(\sum_{j=1}^{n} a_{nj} - \sum_{j=1}^{n} b_{jn}\right) y_n = \frac{K^2}{4}, \end{aligned} \tag{A6}$$

which implies that $-\frac{K}{2} \leqslant y_n \leqslant \frac{K}{2}$. Since $y_1 \leqslant y_n \leqslant \frac{K}{2}$ and $y_1 \geqslant \frac{K}{2}$ by hypothesis, we get $y_1 = y_n = \frac{K}{2}$. This obviously leads to the solution $x_1^\star = \cdots = x_n^\star = K$.

This completes the proof of the theorem. ■

Observe that this result is general for connected graphs, irrespective of the specific network structure yielded by matrix M. In other words, we have not made any assumption on the distribution of the links, some of which can be absent (some $a_{ij} = 0$ or $b_{ij} = 0$), to prove that the only equilibrium points are those associated to full infection or to the absence of the infection.

We now focus on the stability of these equilibrium points. It can be shown that the equilibrium point associated to pathogen coexistence across individuals, $\boldsymbol{x}^\star = K\mathbf{1}$, is *globally asymptotically stable*. We proceed as follows: (i) first we show that $\boldsymbol{x}^\star = K\mathbf{1}$ is asymptotically stable; (ii) then we show that the other equilibrium point, $\boldsymbol{x}^\star = \mathbf{0}$, is unstable; and (iii) as the origin is unstable, the global stability of the coexistence equilibrium arises because the state space of feasible solutions is invariant to the dynamical system, which implies that every trajectory with positive initial conditions will converge to $\boldsymbol{x}^\star = K\mathbf{1}$.

The Jacobian matrix can be expressed as $J = D + A$, where D is a diagonal matrix $D = (d_{ii})$ whose diagonal entries are given by

$$d_{ii} = r - \frac{2rx_i^\star}{K} - \sum_{j=1}^{n} b_{ji}. \tag{A7}$$

The stability of the coexistence equilibrium point follows as a corollary of the Gershgorin circle theorem, which we reproduce here for the sake of completeness:

Theorem 2. Let S be a complex $n \times n$ matrix with entries s_{ij}. Let $R_i = \sum_{j \neq i} |s_{ij}|$ be the sum of the absolute values of the nondiagonal entries in the ith row. Let $D(s_{ii}, R_i) \subseteq \mathbb{C}$ be a closed disk centered at s_{ii} with radius R_i (such a disk is called a Gershgorin disk). Then every eigenvalue of S lies within at least one of the Gershgorin disks $D(m_{ii}, R_i)$.

Then, stability follows directly:

Corollary 1. If condition (5) is satisfied, the equilibrium point of Eq. (1) associated to full infection, $x_1^\star = \cdots = x_n^\star = K$, is asymptotically stable.

Proof. The Jacobian matrix, in this case, reduces to $J = D + A$ with $d_{ii} = -r - \sum_j b_{ji}$. The Gershgorin circle theorem helps show that all the eigenvalues of J have a strictly negative real part. Indeed, for each row of J, the radius of the ith disk is $R_i = \sum_j a_{ij}$ because $a_{ij} \geqslant 0$. Therefore, each disk $D(-r - \sum_j b_{ji}, \sum_j a_{ij})$ is centered on the real axis, and each one is contained in the complex semiplane $\mathrm{Re}\, z \leqslant -r$, because the right-most point of the disk is the real number $-r - \sum_j b_{ji} + \sum_j a_{ij} = -r$. Thus, any eigenvalue satisfies $\mathrm{Re}\,\lambda \leqslant -r$ and has a strictly negative real part. Hence the equilibrium point is asymptotically stable. ■

Again, this result is independent of whether matrices A and B have an adjacency matrix M superimposed or not. It is general as long as the condition of per-capita flux balance, Eq. (5), holds.

On the other hand, we can show that the equilibrium point associated to pathogen clearance, $\boldsymbol{x}^\star = \mathbf{0}$, is unstable. We state this as a proposition:

Proposition 1. If condition (5) holds, the equilibrium point of Eq. (1) associated to full pathogen extinction, $x_1^\star = \cdots = x_n^\star = 0$, is unstable.

Proof. The Jacobian matrix has diagonal entries given by $d_{ii} = r - \sum_j b_{ji}$. Then trivially the vector $\mathbf{1}^T$ is an eigenvector of J with eigenvalue r, because $\sum_j J_{ij} = d_{ii} + \sum_j a_{ij} = r + \sum_j a_{ij} - \sum_j b_{ji} = r$. As J has constant row sums, then $\mathbf{1}$ is an eigenvector with eigenvalue equal to each row sum. Because there is an eigenvalue with a strictly positive real part, this point is unstable, as stated. ■

To finish with the qualitative analysis, we need to rule out the possibility that trajectories do not cross the boundaries of the space of feasible solutions, $x_i = 0$, $i = 1, \ldots, n$. But it is easy to check that any trajectory starting with initial condition $\boldsymbol{x}(0)$ in the interior of the space $\mathbb{R}^n_+ = \{\boldsymbol{x} \in \mathbb{R}^n | x_i \geqslant 0, i = 1, \ldots, n\}$ remains in that space; i.e., the space of feasible solutions is invariant. We state this as a proposition:

Proposition 2. The state space of feasible solutions associated to Eq. (1), $\mathbb{R}^n_+$, is invariant.

Proof. First consider the initial condition $\boldsymbol{x}(0) = \mathbf{0}$. Since $\boldsymbol{x} = \mathbf{0}$ is an equilibrium point, the trajectory remains in $\mathbb{R}^n_+$.

Now consider an initial condition such that $x_i(0) \geqslant 0$ for all $i = 1, \ldots, n$ and some of the initial values verify $x_j(0) > 0$. Then it is easy to see that $x_i(t) \geqslant 0$ for all $t > 0$ and all $i = 1, \ldots, n$. Assume that some variable $x_k(t_a) = 0$ vanishes at $t = t_a > 0$. At that time it holds that

$$\left.\frac{dx_k}{dt}\right|_{t=t_a} = \sum_{s=1}^{n} a_{ks} x_s(t_a) \geqslant 0. \tag{A8}$$

Because the derivative is non-negative, the flux of the ordinary differential equations (ODE) system does not allow the trajectory to cross the axis $x_k = 0$. The same holds for the remaining variables. Hence any initial condition $\boldsymbol{x}(0) \in \mathbb{R}^n_+$ yields a trajectory contained in the state space of feasible solutions. ■

This proposition, together with Corollary 1 and Proposition 1, yields the following corollary:

Corollary 2. If condition (5) is satisfied, the equilibrium point of Eq. (1) associated to full infection, $x_1^\star = \cdots = x_n^\star = K$, is globally asymptotically stable.

Proof. This follows trivially because the state space $\mathbb{R}^n_+$ is invariant and the unique stable equilibrium point is $\boldsymbol{x}^\star = K\mathbf{1}$. Hence all trajectories will converge to $\boldsymbol{x}^\star = K\mathbf{1}$ and its basin of attraction will be $\mathbb{R}^n_+ - \{\mathbf{0}\}$, i.e., the full state space except the unstable equilibrium point. ■

APPENDIX B: STABILITY RESULTS FOR THE GENERAL CASE

The behavior described in Appendix A for the flux-balanced model is recovered *almost surely* if no restrictions are imposed in matrices A and B. Regarding the system's equilibria, it is always found to be the one associated to pathogen clearance, $\boldsymbol{x}^\star = \mathbf{0}$. According to the results provided below in this Appendix, it is very likely that an equilibrium point associated to full infection, $\boldsymbol{x}^\star$ with $x_i^\star > 0$ for $i = 1, \ldots, n$,

exists. But, if the network is connected, no equilibria can arise that combine infected and healthy individuals *almost surely*:

Proposition 3. Consider the dynamics (1) with unrestricted, random per-capita flux matrices A and B (with independent and identically distributed entries). If the adjacency matrix M defines a connected graph, almost surely no equilibrium points $\boldsymbol{x}^\star$ exist such that some pathogen abundances are positive and some of them are exactly equal to zero.

Proof. Assume, without loss of generality, that the first k abundances of $\boldsymbol{x}^\star$ are equal to zero, $x_1^\star = \cdots = x_k^\star = 0$, and the remaining ones are positive, $x_i^\star > 0$ for $i = k+1, \ldots, n$. Then Eq. (A1) reduces, for $i = 1, \ldots, k$, to

$$\sum_{j=k+1}^{n} a_{ij} x_j^\star = 0. \tag{B1}$$

Let A_1 be the submatrix of A formed by the columns from $j = k+1$ to $j = n$ and the rows from $i = 1$ to $i = k$. Then if Eq. (B1) was true, this would imply that the random matrix A_1 is not full rank. But this is a contradiction because any (connected) random matrix is full rank (see Corollary 1.2 in Ref. [39]).

Observe that, if the graph were disconnected, then we could find equilibria with nonzero entries within one or more connected components and zero entries in other components. Equation (B1) would not impose any restriction because matrix elements $a_{ij} = 0$ between disconnected components. For example, if infection spreading starts in a node within a component, at the end this component will reach a fully infected state, whereas the remaining components will have healthy individuals. ■

Therefore, we can expect *almost surely* that the only equilibrium points of Eq. (1) with unrestricted, random per-capita flux matrices A and B are either $\boldsymbol{x}^\star = \boldsymbol{0}$ or $\boldsymbol{x}^\star$ with all entries $x_i^\star > 0$ for $i = 1, \ldots, n$, if the latter is found as solution of Eq. (A1). This is similar to what we found analytically in Appendix A for the balanced case. In principle, more than one single equilibrium associated to full infection with all $x_i^\star > 0$ could arise. In practice, the majority of realizations should exhibit only the two aforementioned equilibria, as in the balanced case. Observe that this applies to the conservative case, because it is a particular case of the unrestricted flux situation.

Can we say something about the stability of these two equilibria? The following proposition holds:

Proposition 4. Let $\boldsymbol{x}^\star = (x_i^\star)$ be a solution of Eq. (A1), and let

$$J(\boldsymbol{x}^\star) = diag\left(r - \frac{2rx_i^\star}{K} - \sum_{j=1}^{n} b_{ji}\right) + A \tag{B2}$$

be the Jacobian matrix evaluated at that equilibrium point, where $diag(\boldsymbol{u})$ stands for a diagonal matrix defined by vector $\boldsymbol{u}$. Then, if the full infection equilibrium $\boldsymbol{x}^\star$ ($x_i^\star > 0$) exists, it holds that

$$(J(\boldsymbol{x}^\star)\boldsymbol{x}^\star)_i = -\frac{rx_i^{\star 2}}{K}, \tag{B3}$$

for $i = 1, \ldots, n$. Moreover, if the full infection equilibrium arises, at the full pathogen's clearance equilibrium we find that

$$(J(\boldsymbol{0})\boldsymbol{x}^\star)_i = \frac{rx_i^{\star 2}}{K}, \tag{B4}$$

for $i = 1, \ldots, n$ and $\boldsymbol{x}^\star$ the full pathogen infection equilibrium point.

Proof. It is easy to compute that

$$\begin{aligned}(J(\boldsymbol{x}^\star)\boldsymbol{x}^\star)_i &= rx_i^\star - \frac{2rx_i^{\star 2}}{K} - x_i^\star \sum_{j=1}^{n} b_{ji} + (A\boldsymbol{x}^\star)_i \\ &= -\frac{rx_i^{\star 2}}{K} + rx_i^\star - \frac{rx_i^{\star 2}}{K} - x_i^\star \sum_{j=1}^{n} b_{ji} + (A\boldsymbol{x}^\star)_i,\end{aligned} \tag{B5}$$

but in the last equality all the terms except the first vanish because $\boldsymbol{x}^\star$ is a solution of Eq. (A1). Similarly,

$$\begin{aligned}(J(\boldsymbol{0})\boldsymbol{x}^\star)_i &= rx_i^\star - x_i^\star \sum_{j=1}^{n} b_{ji} + (A\boldsymbol{x}^\star)_i \\ &= \frac{rx_i^{\star 2}}{K} + rx_i^\star - \frac{rx_i^{\star 2}}{K} - x_i^\star \sum_{j=1}^{n} b_{ji} + (A\boldsymbol{x}^\star)_i,\end{aligned} \tag{B6}$$

and we get Eq. (B4). ■

Expressions (B3) and (B4) can be used to provide accurate approximations of the rightmost eigenvalue of the Jacobian matrix for both equilibria. If $\boldsymbol{v} = (v_i)$ was an eigenvector of J, we would have that $(J(\boldsymbol{x}^\star)\boldsymbol{v})_i = \lambda v_i$. If all entries are real and $v_i > 0$, then we could write λ as

$$\lambda = \frac{1}{n} \sum_{i=1}^{n} \frac{(J(\boldsymbol{x}^\star)\boldsymbol{v})_i}{v_i}. \tag{B7}$$

Numerically we find that the eigenvector $\boldsymbol{v}$ associated with the eigenvalue that determines stability can be approximated by $\boldsymbol{x}^\star$, if this full infection equilibrium point exists. Then Eqs. (B3) and (B4) can be written as

$$\frac{1}{n} \sum_{i=1}^{n} \frac{(J(\boldsymbol{x}^\star)\boldsymbol{x}^\star)_i}{x_i^\star} = -\frac{r}{K}\overline{\boldsymbol{x}^\star} \tag{B8}$$

and

$$\frac{1}{n} \sum_{i=1}^{n} \frac{(J(\boldsymbol{0})\boldsymbol{x}^\star)_i}{x_i^\star} = \frac{r}{K}\overline{\boldsymbol{x}^\star}, \tag{B9}$$

respectively. Here $\overline{\boldsymbol{v}} := \frac{1}{n}\sum_{i=1}^{n} v_i$. If the full infection equilibrium exists and the approximation for the eigenvector $\boldsymbol{v} \approx \boldsymbol{x}^\star$ is correct, then the right-most eigenvalue can be approximated by $-\frac{r}{K}\overline{\boldsymbol{x}^\star}$ for the full infection equilibrium (which will be stable), and by $\frac{r}{K}\overline{\boldsymbol{x}^\star}$ for the full pathogen clearance (which, as a consequence, will be unstable). Figure 7 shows the goodness of such approximations for ER networks with different connectivity values. We observe that the approximation works better for increasing values of the connection probability p, yielding an almost perfect agreement in the limit $p \to 1$.

We conclude that, in situations where these two equilibrium points appear, the one associated to full infection is stable, and the one associated to pathogen clearance is not.

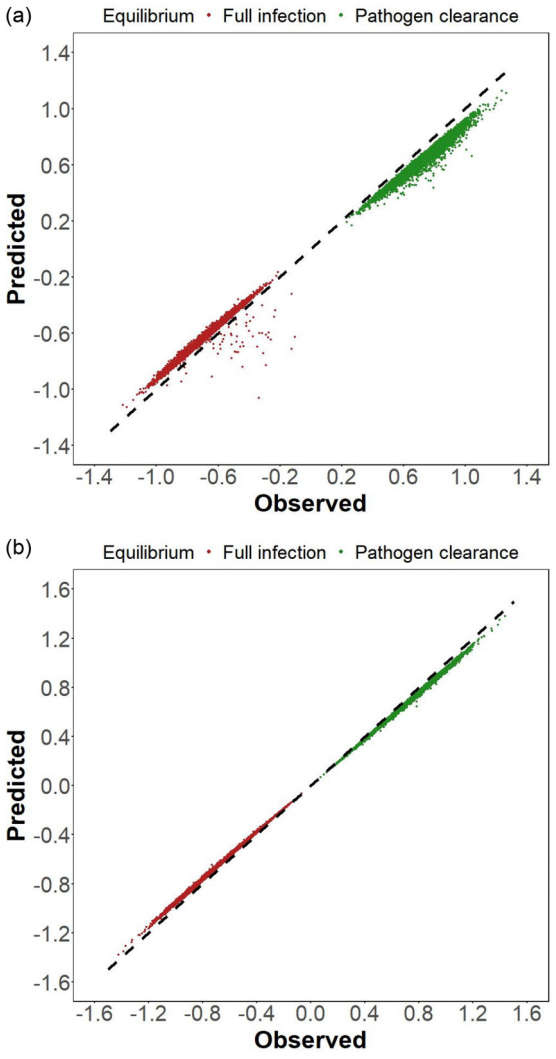

FIG. 7. Predicted and observed eigenvalues. Observed rightmost eigenvalue of the Jacobian matrix (B2) at $\boldsymbol{x}^\star = \mathbf{0}$, together with predicted values given by Eq. (B4) (green dots). Red dots stand for predicted [cf. Eq. (B3)] vs observed stability eigenvalues at the full infection equilibrium point, in realizations where both equilibria coexist. A total of 10^4 Erdős-Rényi model network realizations ($n = 100$ nodes) were taken to produce both panels. (a) $p = 0.1$ and (b) $p = 0.2$; both values are well above the percolation threshold. As p approaches 1, the agreement between predicted and observed becomes almost perfect.

In summary, the qualitative behavior of critical points in the general case is very similar to the case of per-capita flux balance.

To finish the qualitative analysis of the general model, we have studied the effect of network connectivity in ER graphs on the stability of the two equilibria that can appear in this case. We provide the results of this exploration in Fig. 8.

We observe that, for small mean degrees (in particular, for those reported in Fig. 2), the full infection equilibrium is always stable and the pathogen clearance is unstable. However, for largely connected networks, in some cases the latter equilibrium becomes stable—in which cases the coexistence equilibrium does not exist. This is more apparent for fully

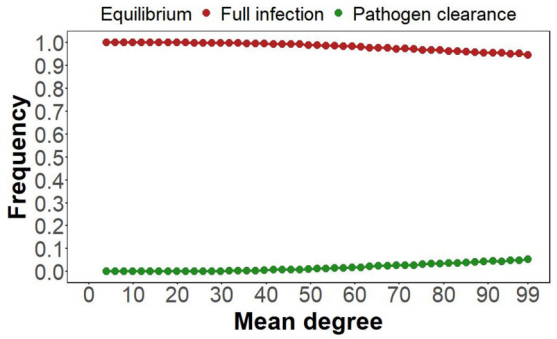

FIG. 8. Probability of stability of the full infection and pathogen clearance equilibria as a function of the expected mean degree. Ten thousand ER model realizations ($n = 100$) were calculated for each connection probability p, and we estimated probabilities as observed frequencies for each equilibrium. As $\mathrm{E}[k] = (n-1)p$ increases, the equilibrium $\boldsymbol{x}^\star = \mathbf{0}$ becomes more likely to be asymptotically stable.

connected networks, for which about a 5% of the realizations yield pathogen clearance as an end state. It is worth mentioning that the sum of the two probabilities is numerically equal to 1, so we did not find additional equilibria across all the realizations.

APPENDIX C: SMALL-WORLD NETWORKS

In this contribution, we have shown that mortality peaks at intermediate network connectivity values, and this phenomenon can be ascribed to the potential fragmentation of the network as infection spreads. However, not every model of random network formation exhibits a percolation transition due to the formation of a giant component. According to our results, in this case the maxima should not appear.

Figure 9 summarizes simulation results for our epidemic spreading dynamics of the WS model for small-world network structure [compare these results with those reported in Fig. 2(c)]. As the WS model generates connected networks, infection spreads throughout the network for any value of the mean degree. This explains that no maximum is observed in plant mortality.

APPENDIX D: ROBUSTNESS OF RESULTS

We carried out additional simulations to test the robustness of our main result, i.e., the existence of a peak in the number of dead plants as the network's average degree increases. We analyze three variations of our model: (i) one that incorporates variability in the death threshold δ, (ii) the case in which flux matrices A and B do not have the same mean value, and (iii) the case in which pathogenic concentrations in dead individuals are taken into account and can effectively contribute to infection across the system after an individual's death. In these three robustness tests, we use ER network structures to conduct simulations.

In the first test, we incorporate variability in δ to allow for a specific pathogen's tolerance for each individual. We drew n values δ_i from a normal distribution $\mathcal{N}(0.9K, 0.1K)$ checking that no one of them was negative. We kept these values fixed across simulations, where we averaged over realizations of

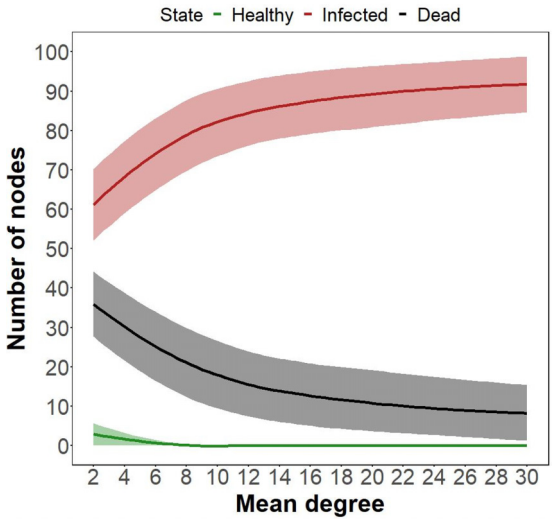

FIG. 9. Small-world networks. Here the fraction of healthy, infected, and dead nodes is represented as function of the mean degree of network samples of the WS model—notice that the minimum possible average degree in this model is $\mathrm{E}[k] = 2$. Because model networks are connected, we observe no maximum in the number of dead nodes. We used a rewiring probability $\phi = 0.01$ to generate WS model networks. Parameter values for r, K, and δ are the same as in Fig. 2. We averaged over 1200 realizations.

matrices A and B, as in Sec. II. Figure 10 shows how the fractions of healthy, infected, and dead plants vary with mean degree.

As shown in Fig. 10, our results remain robust to this modification: the shape of each average's curve is maintained, although there is more variability than for the constant-δ model.

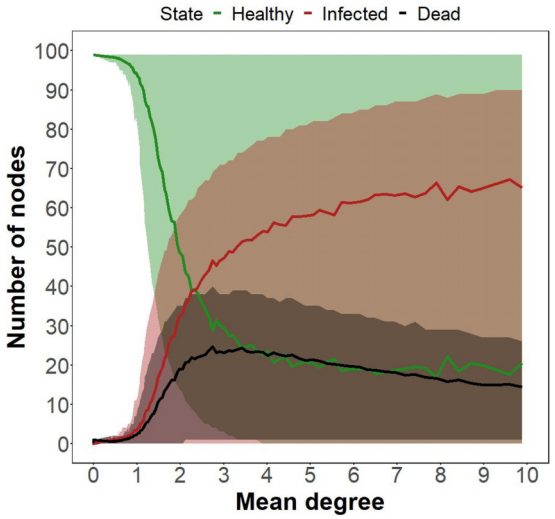

FIG. 10. Variable mortality threshold. Fraction of individuals within compartments, as a function of network mean degree (ER), when the mortality threshold is plant dependent and drawn from a distribution. Here values of δ_i were drawn at the beginning of the simulation, and averages were taken over flux matrices A and B.

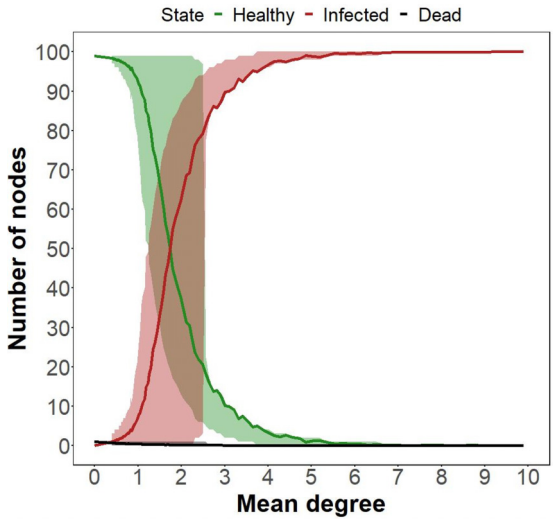

FIG. 11. Different means in transport matrices. Fraction of individuals within compartments, as a function of network mean degree (ER), when $a_{ij} \sim U[0, 1]$ and $b_{ij} = a_{ij} + U[0, 1]$. This is a possible way to ensure that $b_{ij} \geqslant a_{ij}$, so that pathogen losses occur across each link. Remaining parameters are maintained as in Fig. 2.

The second modification we have considered is the case of different means for transport matrices A and B. Our model is flexible enough to model situations in which fluxes are not necessarily equally distributed. The simplest way to take this into account is by considering different averages in matrices A and B. For example, a particular scenario with different means would be considering pathogen losses across links by imposing $B \geqslant A$ component-wise. Below we show results of the proportion of healthy, infected, and dead nodes when $a_{ij} \sim U[0, 1]$ and $b_{ij} = a_{ij} + U[0, 1]$, one of the possible ways of ensuring that $B \geqslant A$. These results are presented in Fig. 11.

The actual average fraction of dead nodes in the case of different means depends on the relative balance between the difference of means, $|\langle A\rangle - \langle B\rangle|$, and the death threshold. For the case shown in Fig. 11, $\langle A\rangle = \frac{1}{2}$ and $\langle B\rangle = 1$. Here the flux of pathogen losses across links is high enough for most of the plants not reaching the death threshold, resulting in almost a complete reduction of plant mortality. Lowering the death threshold but keeping these means unbalanced can increase the fraction of dead nodes as in the case of equal means, leading to a peak in mortality. Additionally, if a smaller mean difference between fluxes is chosen, the maximum in plant mortality arises again.

The third extension of our model considers the dynamics of remaining pathogen after an individual's death. In the main text, we basically ignore the pathogen that remains in dead plants as able to infect other individuals, but in reality it can be transported to other individuals and increase their pathogen load. A reasonable way to model pathogen dynamics once the host plant is dead is by releasing out pathogen concentration, so that the remaining pathogen in dead hosts decays exponentially at rate α, because pathogen reproduction will be hindered due to the lack of healthy tissues in the plant. This concentration is obviously nonzero until some relaxation

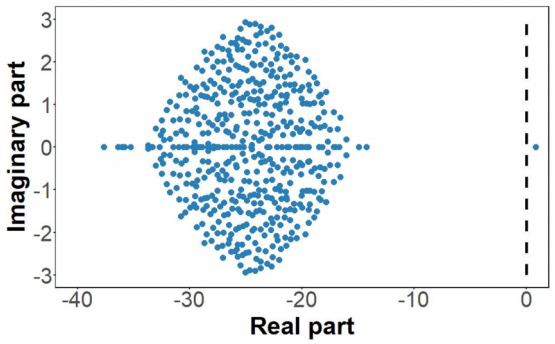

FIG. 12. Eigenvalue spectrum of the Jacobian matrix of the dynamical model (1) modified by Eq. (D1) to account for pathogen in dead nodes. Here, we show the spectrum for an ER model realization with $\alpha = 1, r = 0.5, K = 1, n = 500$, and $p = 0.1$, in which we have imposed that 100 plants crossed over the threshold and died; for the qualitative analysis of the interior equilibrium point, the transient dynamics until all deaths have occurred is irrelevant. As shown, an outlier eigenvalue makes the interior equilibrium point unstable; the vertical dashed line marks the line $\mathrm{Re}(\lambda) = 0$. This instability is less likely as α grows.

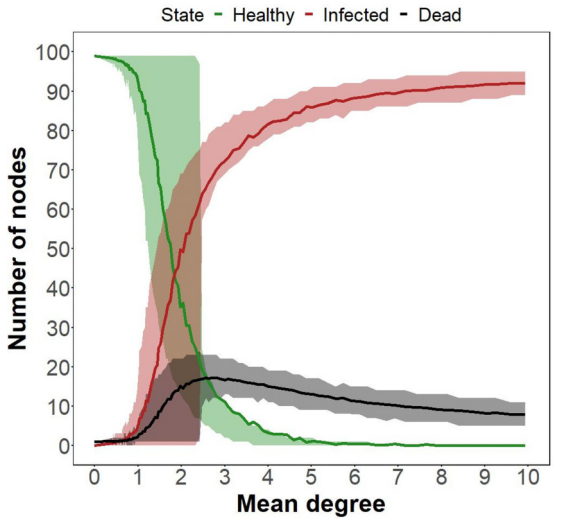

FIG. 13. Fraction of dead plants as a function of network mean degree (ER), when dead plants in simulations can release pathogen to the exterior in a way that the pathogen concentration that remains decreases exponentially with exponent α (here, $\alpha = 10$). Again, averages were taken over flux matrices A and B.

time has elapsed. Therefore, this pathogen is still available to be transported to other nodes.

The dynamical model is modified as follows. The ith equation of the coupled dynamics is given by Eq. (1) for any time t such that $x_i(t) \leqslant \delta$. Let t_i be the time at which plant i crosses over the threshold δ, $x_i(t_i) = \delta$. Then, for $t \geqslant t_i$ the ith equation of (1) is substituted by

$$\frac{dx_i}{dt} = -\alpha x_i + \sum_{j=1}^{n} a_{ij}x_j - x_i \sum_{j=1}^{n} b_{ji}, \text{ for } t \geqslant t_i. \tag{D1}$$

For this modification to be meaningful, the rate α at which pathogen decays in dead nodes has to be large. Otherwise, we can find examples of unstable dynamics (Fig. 12). Intuitively, if α is small (i.e., pathogen concentration decays slowly in dead nodes), the likelihood that the right-hand side of Eq. (D1) becomes positive for a number of nodes is non-negligible, which can lead to unbounded growth in pathogen concentration at some nodes. There must be a critical value above which no unstable equilibria are found. For that reason, this model modification is meaningful in the limit of strong decay. In terms of pathogen population dynamics in dead individuals, this limit is consistent with situations in which healthy tissues in the host are scarce. In principle, the per-capita decay rate α should be a quantity increasing in time because of the increasing lack of resources for pathogen reproduction. Instead of considering an increasing function $\alpha(t)$, we use an asymptotic value large enough to ensure the stability of the dynamics.

Incorporating this effect we observe no qualitative change in our main results. To check this, we have chosen α such that pathogen declines fast enough in dead individuals. These simulations are shown in Fig. 13, demonstrating that our results are robust to this modification: the peak in mortality remains.

APPENDIX E: COMPARISON TO SIR MODELS

The first model that one can think of to effectively describe pathogen dynamics is the standard SIR model (without vital dynamics) [11,40]:

$$\frac{ds}{dt} = -\sigma si, \quad \frac{di}{dt} = \sigma si - i, \quad \frac{dr}{dt} = i,$$

where we have used time units such that the rate γ from infected to removed is equal to 1, and the contact number is precisely the rate σ from susceptible to infected. Here $s(t)$, $i(t)$, and $r(t)$ stand for the fractions of susceptible (healthy), infected, and removed (dead) plants as functions of time. The equations obviously preserve the condition $s(t) + i(t) + r(t) = 1$. It is easy to see, using this model, that asymptotically the fraction of infected individuals goes to zero, irrespective of the initial condition. This is inconsistent with the microscopic temporal dynamics reported in Fig. 4, for which a nonzero fraction of infected individuals remain in the long term—the infection is endemic in our model. Then the standard SIR model has to be ruled out to reproduce effectively our microscopic dynamics.

Next we consider a SIR model with vital dynamics,

$$\frac{ds}{dt} = -\sigma s\, i - \mu s + \mu, \quad \frac{di}{dt} = \sigma s\, i - i - \mu i, \quad \frac{dr}{dt} = i - \mu r, \tag{E1}$$

which still preserves the restriction $s(t) + i(t) + r(t) = 1$ along the dynamics. The difference with a standard SIR model is that each compartment is affected by the same mortality rate μ, which is compensated in the fraction of susceptible individuals, growing as $\frac{ds}{dt} = \mu(1 - s)$ in isolation. It is easy to check that, asymptotically, the fractions in each compartment tend to

$$s^\star = \frac{1+\mu}{\sigma}, \quad i^\star = \frac{\mu}{\sigma}\left(\frac{1}{s^\star} - 1\right), \quad r^\star = \frac{1}{\sigma}\left(\frac{1}{s^\star} - 1\right). \tag{E2}$$

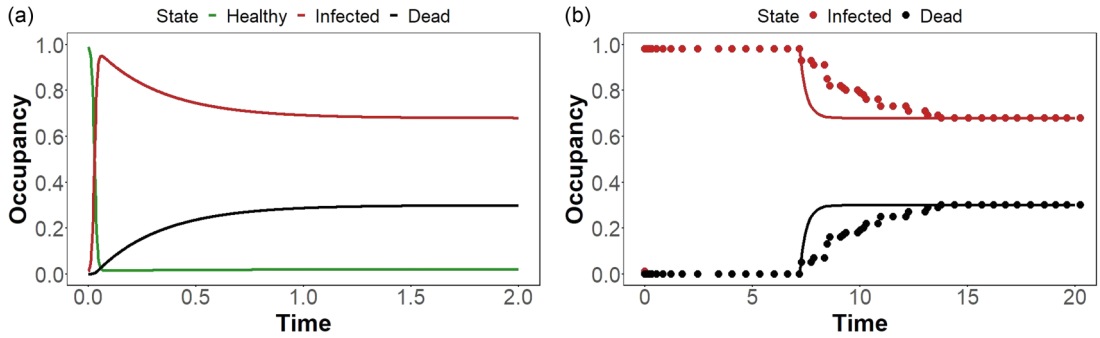

FIG. 14. Fraction of individuals within compartments, for the SIS model (left) and our microscopic approach (right), which corresponds to that depicted on Fig. 4(b). Left: Using the asymptotic values to be adjusted from the simulation in Fig. 4(b), $(s^\star, i^\star, r^\star) = (0.02, 0.68, 0.3)$, we solve Eq. (E2) for σ and μ to get $\mu = \frac{i^\star}{1-s^\star-i^\star} = 2.267$ and $\sigma = \frac{1-s^\star}{s^\star(1-s^\star-i^\star)} = 163.33$. With these parameters, the numerical integration of Eq. (E1) yields the temporal SIR dynamics depicted in the panel. Right: Microscopic model aggregated dynamics (dots) compared with the time-dependent approximations given by Eq. (E4) (solid lines). We have aggregated into compartments the temporal dynamics presented in Fig. 4(b). Here $t_0 \approx 7.189$ and μ remains unchanged in terms of $i^\star$ and $s^\star$. Notice that the intermediate transient observed in the microscopic model until $t = t_0$ has no counterpart in the full SIR model (left).

This solves the problem described above for the standard SIR model, because here it is possible that $i^\star > 0$, as we observe in the microscopic pathogen dynamics. However, for networks exhibiting a giant component [see Figs. 4(b) and 4(c)], it is expected that the fraction of susceptible individuals tends to a low, constant value after a short transient time (equal to zero for fully connected networks). In other words, our microscopic model predicts a fast decrease of the fraction of healthy plants. Therefore, an effective SIR model with vital dynamics will be able to reproduce our microscopic pathogen propagation over almost fully connected networks in the limit $\sigma \to \infty$, because $s(t)$ will decay rapidly to an asymptotic value $s^\star \approx 0$. After that transient, $s(t) \approx s^\star$ is approximately constant, so we can set equal to zero the right-hand side of the equation for s to obtain $\sigma i(t) s^\star = \mu - \mu s^\star$. Substituting into the equation for $i(t)$ we get a system of ODEs where only infected and removed individuals remain (and $s = s^\star$ is kept fixed):

$$\frac{di}{dt} = \mu(1 - s^\star) - (1 + \mu)i, \qquad \frac{dr}{dt} = i - \mu r, \tag{E3}$$

which can be used to predict the dynamics for $t \geqslant t_0$, t_0 being the time at which the fraction of dead individuals $r(t_0)$ starts growing. This system preserves the condition $s^\star + i(t) + r(t) = 1$. Equation (E3) leads to fractions $i^\star = \frac{\mu}{1+\mu}(1 - s^\star)$ and $r^\star = \frac{1-s^\star}{1+\mu} = \mu i^\star$ in the steady state, so we can solve for $\mu = \frac{i^\star}{1-s^\star-i^\star}$ in terms of equilibrium fractions. In this limit, the approximate system becomes linear (and hence trivial), yielding the analytical solution

$$\begin{aligned} i(t) &= i^\star + (i_0 - i^\star)e^{-(t-t_0)(1+\mu)}, \\ r(t) &= r^\star - (i_0 - i^\star)e^{-(t-t_0)(1+\mu)}, \end{aligned} \tag{E4}$$

with initial conditions $i(t_0) = 1 - s^\star$ and $r(t_0) = 0$. Then, the temporal dynamics is fully determined by the asymptotic fractions $i^\star$ and $s^\star$.

We can use the microscopic model's average fractions of infected and dead plants to find parameters values for $\mu = \frac{i^\star}{1-s^\star-i^\star}$ and t_0. First we determine from the simulation the initial time t_0 at which $r(t)$ starts growing. The asymptotic fractions of healthy and infected individuals yield values for $i^\star$ and $s^\star$. Then we can immediately obtain the μ value that reproduces the fractions within compartments in the long run (Fig. 14).

The comparison between the SIR with vital dynamics and the microscopic model's fractions is shown in Fig. 14. Note that the aggregated, microscopic temporal dynamics cannot be accounted for with the two standard compartmentalized models discussed here, because there is a transient period before dead individuals start appearing. In addition, even for $t > t_0$ the adjusted temporal dynamics does not fit properly microscopic model fractions within compartments.

[1] N. Cunniffe, R. Cobb, R. Meentemeyer, D. Rizzo, and C. Gilligan, Modeling when, where, and how to manage a forest epidemic, motivated by sudden oak death in California, Proc. Natl. Acad. Sci. USA **113**, 201602153 (2016).

[2] N. Grünwald, J. Leboldus, and R. Hamelin, Ecology and evolution of the sudden oak death pathogen *Phytophthora ramorum*, Annu. Rev. Phytopathol. **57**, 301 (2019).

[3] K. Schneider, W. van der Werf, M. Cendoya, M. Mourits, J. A. Navas-Cortés, A. Vicent, and A. Oude Lansink, Impact of *Xylella fastidiosa* subspecies *pauca* in European olives, Proc. Natl. Acad. Sci. USA **117**, 9250 (2020).

[4] R. Anderson, C. Fraser, A. Ghani, C. Donnelly, S. Riley, N. Ferguson, G. Leung, T. Lam, and A. Hedley, Epidemiology, transmission dynamics and control of SARS: The 2002-2003 epidemic, Philos. Trans. R. Soc. B **359**, 1091 (2004).

[5] N. Ferguson, C. Donnelly, and R. Anderson, The foot-and-mouth epidemic in Great Britain: Pattern of spread and impact of interventions, Science **292**, 1155 (2001).

[6] N. Ferguson, C. Donnelly, and R. Anderson, Erratum: Transmission intensity and impact of control policies on the foot and mouth epidemic in Great Britain, Nature (London) **413**, 542 (2001).

[7] R. May and R. Anderson, Population biology of infectious diseases: Part II, Nature (London) **280**, 455 (1979).

[8] C. Hens, U. Harush, S. Haber, R. Cohen, and B. Barzel, Spatiotemporal signal propagation in complex networks, Nat. Phys. **15**, 403 (2019).

[9] E. Estrada, S. Meloni, M. Sheerin, and Y. Moreno, Epidemic spreading in random rectangular networks, Phys. Rev. E **94**, 052316 (2016).

[10] M. Keeling and K. Eames, Networks and epidemic models, J. R. Soc. Interface **2**, 295 (2005).

[11] R. M. Anderson and R. M. May, *Infectious Diseases of Humans: Dynamics and Control* (Oxford University Press, Oxford, U.K., 1992).

[12] J. Li, H.-J. Duan, H.-Y. Chen, Y.-J. Ji, X. Zhang, Y.-H. Rong, Z. Xu, L.-J. Sun, J.-Y. Zhang, L.-M. Liu *et al.*, Age and Ebola viral load correlate with mortality and survival time in 288 Ebola virus disease patients, Int. J. Infect. Dis. **42**, 34 (2016).

[13] E. Pujadas, F. Chaudhry, R. McBride, F. Richter, S. Zhao, A. Wajnberg, G. Nadkarni, B. S. Glicksberg, J. Houldsworth, and C. Cordon-Cardo, SARS-CoV-2 viral load predicts COVID-19 mortality, Lancet Respir. Med. **8**, e70 (2020).

[14] J. Dormans, M. Burger, D. Aguilar, R. Hernandez-Pando, K. Kremer, P. Roholl, S. Arend, and D. Van Soolingen, Correlation of virulence, lung pathology, bacterial load and delayed type hypersensitivity responses after infection with different *Mycobacterium tuberculosis* genotypes in a BALB/c mouse model, Clin. Exp. Immunol. **137**, 460 (2004).

[15] N. J. Grünwald, E. M. Goss, and C. M. Press, *Phytophthora ramorum*: A pathogen with a remarkably wide host range causing sudden oak death on oaks and ramorum blight on woody ornamentals, Mol. Plant Pathol. **9**, 729 (2008).

[16] N. J. Grünwald, M. Garbelotto, E. M. Goss, K. Heungens, and S. Prospero, Emergence of the sudden oak death pathogen *Phytophthora ramorum*, Trends Microbiol. **20**, 131 (2012).

[17] M. Keeling, The implications of network structure for epidemic dynamics, Theor. Popul. Biol. **67**, 1 (2005).

[18] C. Castellano and R. Pastor-Satorras, Thresholds for Epidemic Spreading in Networks, Phys. Rev. Lett. **105**, 218701 (2010).

[19] J. A. Cuesta, J. Aguirre, J. A. Capitán, and S. C. Manrubia, Struggle for Space: Viral Extinction through Competition for Cells, Phys. Rev. Lett. **106**, 028104 (2011).

[20] J. A. Capitán, J. A. Cuesta, S. C. Manrubia, and J. Aguirre, Severe hindrance of viral infection propagation in spatially extended hosts, PLoS One **6**, e23358 (2011).

[21] C. Stegehuis, R. Van Der Hofstad, and J. S. Van Leeuwaarden, Epidemic spreading on complex networks with community structures, Sci. Rep. **6**, 29748 (2016).

[22] M. De Domenico, C. Granell, M. A. Porter, and A. Arenas, The physics of spreading processes in multilayer networks, Nat. Phys. **12**, 901 (2016).

[23] S. Bansal, B. T. Grenfell, and L. A. Meyers, When individual behaviour matters: Homogeneous and network models in epidemiology, J. R. Soc. Interface **4**, 879 (2007).

[24] P. Erdös and A. Rényi, On random graphs I, Publ. Math. Debrecen. **6**, 290 (1959).

[25] A. Antonioni and M. Tomassini, Degree correlations in random geometric graphs, Phys. Rev. E **86**, 037101 (2012).

[26] M. Penrose, *Random Geometric Graphs* (Oxford University Press, Oxfod, U.K., 2003).

[27] E. Estrada, *The Structure of Complex Networks: Theory and Applications* (Oxford University Press, Oxford, U.K., 2012).

[28] D. J. Watts and S. H. Strogatz, Collective dynamics of 'small-world' networks, Nature (London) **393**, 440 (1998).

[29] C. A. Serván, J. A. Capitán, J. Grilli, K. E. Morrison, and S. Allesina, Coexistence of many species in random ecosystems, Nat. Ecol. Evol. **2**, 1237 (2018).

[30] S. Allesina and S. Tang, Stability criteria for complex ecosystems, Nature (London) **483**, 205 (2012).

[31] I. Hanski, Metapopulation dynamics, Nature (London) **396**, 41 (1998).

[32] R. Mukherjee, H. A. Gruszewski, L. T. Bilyeu, D. G. Schmale, and J. B. Boreyko, Synergistic dispersal of plant pathogen spores by jumping-droplet condensation and wind, Proc. Natl. Acad. Sci. USA **118**, e2106938118 (2021).

[33] X. Xu, T. D. Harwood, M. Pautasso, and M. J. Jeger, Spatio-temporal analysis of an invasive plant pathogen (*Phytophthora ramorum*) in England and Wales, Ecography **32**, 504 (2009).

[34] R. Pastor-Satorras, C. Castellano, P. Van Mieghem, and A. Vespignani, Epidemic processes in complex networks, Rev. Mod. Phys. **87**, 925 (2015).

[35] R. Pastor-Satorras and A. Vespignani, Epidemic dynamics in finite size scale-free networks, Phys. Rev. E **65**, 035108(R) (2002).

[36] K. A. Schmidt and R. S. Ostfeld, Biodiversity and the dilution effect in disease ecology, Ecology **82**, 609 (2001).

[37] Wildflower plant database, University of Texas, https://www.wildflower.org/plants/ (2021).

[38] S. Werres, R. Marwitz, W. A. M. In't Veld, A. W. De Cock, P. J. Bonants, M. De Weerdt, K. Themann, E. Ilieva, and R. P. Baayen, *Phytophthora ramorum* sp. nov., a new pathogen on rhododendron and viburnum, Mycol. Res. **105**, 1155 (2001).

[39] X. Feng and Z. Zhang, The rank of a random matrix, Appl. Math. Comput. **185**, 689 (2007).

[40] H. W. Hethcote, Three basic epidemiological models, in *Applied Mathematical Ecology* (Springer, Berlin, 1989), pp. 119–144.